Journal of Sound and Vibration (2002) **253**(3), 631–652
doi:10.1006/jsvi.2001.4067, available online at http://www.idealibrary.com on IDEAL®

FREE VIBRATION ANALYSIS OF CANTILEVER PLATES WITH STEP DISCONTINUITIES IN PROPERTIES BY THE METHOD OF SUPERPOSITION

D. J. GORMAN

Department of Mechanical Engineering, University of Ottawa, 770 King Edward Avenue, Ottawa, Ontario, Canada K1N 6N5

AND

R. SINGHAL

Mgr. Structural Qualification Facilities, David Florida Laboratory, Canadian Space Agency, 3701 Carling Ave., Ottawa, Ontario, Canada K2H 8S2

(*Received* 3 *April* 2001, *and in final form* 24 *October* 2001)

Utilizing the superposition method, an analytical type solution is obtained for the free vibration eigenvalues and mode shapes of a cantilever plate with step discontinuities in plate properties. Property discontinuity lines run parallel to the clamped edge of the plate. Verification tests are performed for limiting cases by comparing computed eigenvalues with known eigenvalues for plates with uniform properties. Very good agreement is also obtained when computed results are compared with those obtained experimentally utilizing a test plate with discontinuities in thickness. Computed eigenvalues and mode shapes are presented for the benefit of other researchers. Besides the general interest, the problem has an application in the modelling of certain multi-story buildings during seismic studies.

1. INTRODUCTION

An interest in free vibration analysis of rectangular cantilever plates with step discontinuities in properties has risen in connection with determining the seismic response of certain families of high-rise buildings. It is found that long, narrow, multi-story office or apartment buildings can be modelled, at least initially, by vertical cantilever plates the lower edge being fixed and corresponding to the base of the structure.

Buildings of this type, in general, have a diminishing effective transverse stiffness, as one moves upward, and possibly changes in mass associated with each story. In order to model these changes in the properties of actual structures, the cantilever plate is assigned corresponding effective values of flexural stiffness and mass distribution for the various building stories being modelled. This leads to the step discontinuities in properties (stiffness and mass distribution) as one moves along the plate.

A considerable interest in the vibration of stepped circular plates has existed over the years in connection with their use as ultrasonic radiators. Most of the progress in this area was reviewed by San Emeterio *et al.* [1] in the 1987 paper. Progress in the study of stepped rectangular plates, or plates with discontinuities in properties, has advanced at a much slower rate.

Harik *et al.* [2] have made a study of rectangular plates with intermediate flexible supports utilizing the analytical strip method. They have pointed out that their approach can be utilized to solve a limited class of problems involving rectangular plates with

0022-460X/02/$35.00

discontinuities in thickness. Computed results are presented for the fundamental frequency of a simply supported plate with a single-step discontinuity in thickness. These results are compared with what are usually approximate results obtained by earlier researchers. Again, a fairly complete listing of earlier research work in this area is reported.

A significant paper by Jinkyo and Bergman was published in 1993 [3]. They begin by pointing out that "there are few publications available on the vibration of plates with non-uniform thickness". Nevertheless, they also have a fairly comprehensive review of pertinent literature available up to that time, observing also that most previous work was approximate in nature. Their work was devoted to stepped plates; however, it was strictly limited to plates with at least two opposite simply supported edge. It is known that Levy type solutions can be obtained for this very limited class of problems.

In a follow-up paper, Lee and Bergman described a more general dynamic flexibility method for analyzing the forced and free vibrations of both beams and plates with stepped discontinuities [4]. Again, their plate computations were restricted to cases of plates with at least one pair of opposite edges simply supported. A valuable contribution of this paper was the listing of 44 related references.

Liu and Liew [5] have published a fairly recent paper dealing with the vibration of discontinuous Mindlin plates. They utilized a modified version of a numerical procedure known as the "differential quadrature element method". Their work is mainly relevant here in that it contains a literature review extending from 1963 to 1998.

In this paper, an accurate analytical type solution is obtained for the free vibration frequencies and mode shapes of cantilever plates of the type described above. Following the established procedures, each uniform segment of the plate is analyzed by means of a set of building blocks (forced vibration solutions). Driving coefficients associated with these building blocks are constrained in such a way that all boundary conditions related to the segment as well as conditions of continuity with neighboring segments are satisfied. While the present investigation pertains to cantilever plates, it becomes obvious to the reader that with the superposition of appropriate Levy type solutions (building blocks), the analysis is applicable to plates with any combination of classical boundary conditions. Furthermore, lines of discontinuity may run perpendicular to any pair of opposite edges.

It is also pointed out that the present paper is quite general in that it handles plates with stepped discontinuities in stiffness and mass distribution properties. Plates with discontinuities in thickness constitute only one family of problems which can be handled. It is of no consequence in the present analysis as to how these discontinuities come about. They could be the result of joining plates of identical thickness but different stiffnesses or mass distributions. Such plates could be the result of joining plates of dissimilar metals etc. Also, plates partially covered with uniformly distributed masses can be readily handled. Any degree of accuracy can be achieved in the analysis by increasing the number of terms utilized in the building block solutions. This is also, to the knowledge of the authors, the first paper on the subject to include experimental results.

The objectives set forth here are to familiarize the reader with the method of analysis and to present results of a limited number of illustrative as well as experimental studies.

2. ANALYTICAL PROCEDURE

2.1. DEVELOPMENT OF THE BASIC BUILDING BLOCK SOLUTIONS

Before presenting the over-all arrangement of the building blocks to be deployed in resolving the problem of ultimate interest, it is advantageous to review solutions for the basic building blocks utilized in the analysis.

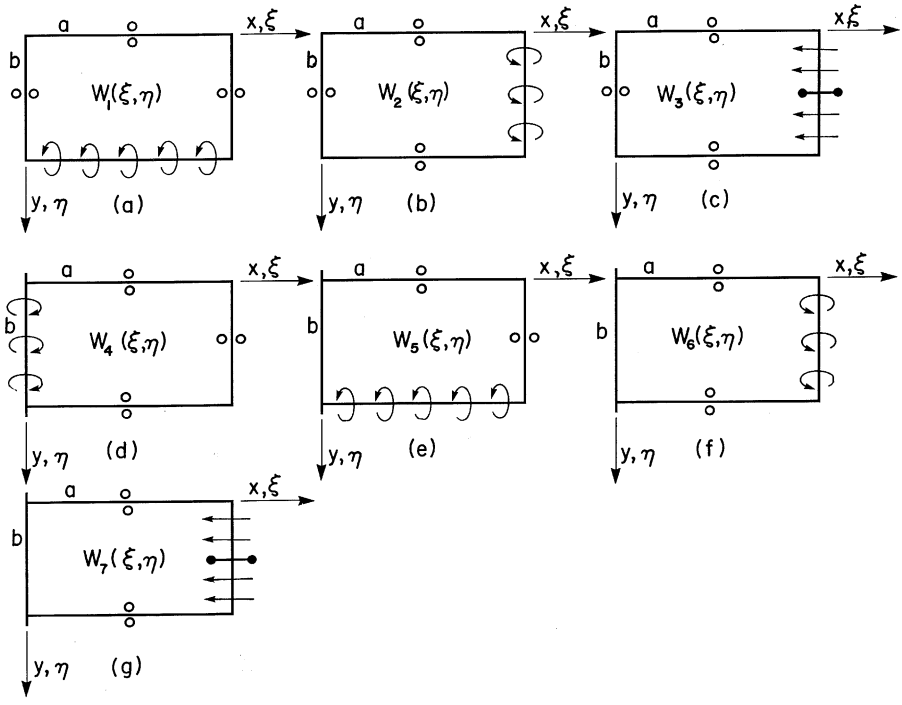

Figure 1. Schematic representation of building blocks utilized in plate analysis.

Consider the first building block, represented schematically in Figure 1, and designated by the symbol (a). Co-ordinates ξ and η represent the distances along the x and y directions divided by edge lengths a and b respectively. Small open circles adjacent to an edge indicate slip–shear boundary conditions, i.e., vertical edge reaction, and slope taken normal to the edge, are zero everywhere. The edge, $\eta = 1$, is free of vertical edge reaction and is driven by a distributed, forced harmonic edge rotation of circular frequency ω.

It is known that a Levy type solution can be written for the spatial response of this building block. It is written as

$$W_1(\xi, \eta) = \sum_{m=0,1}^{\infty} Y_m(\eta) \cos m\pi\xi, \tag{1}$$

where $W_1(\xi, \eta)$ equals the dimensionless lateral displacement w/a.

The differential equation governing vibratory behavior of thin rectangular plates in dimensionless form is expressed as [6]

$$\frac{\partial^4 W(\xi, \eta)}{\partial \eta^4} + 2\phi^2 \frac{\partial^4 W(\xi, \eta)}{\partial \eta^2 \partial \xi^2} + \phi^4 \frac{\partial^4 W(\xi, \eta)}{\partial \xi^4} - \phi^4 \lambda^4 W(\xi, \eta) = 0. \tag{2}$$

Substituting equation (1) into this equation, and separating variables, it is shown that we may write for the function $Y_m(\eta)$,
for $\lambda^2 > (m\pi)^2$,

$$Y_m(\eta) = A_m \cosh \beta_m \eta + B_m \sinh \beta_m \eta + C_m \cos \gamma_m \eta + D_m \sin \gamma_m \eta \tag{3}$$

and for $\lambda^2 < (m\pi)^2$,

$$Y_m(\eta) = A_m \cosh \beta_m \eta + B_m \sinh \beta_m \eta + C_m \cosh \gamma_m \eta + D_m \sinh \gamma_m \eta, \tag{4}$$

where $\beta_m^2 = \phi^2\{\lambda^2 + (m\pi)^2\}$, $\gamma_m^2 = \phi^2\{\lambda^2 - (m\pi)^2\}$ or $\phi^2\{(m\pi)^2 - \lambda^2\}$, whichever is positive. A_m, B_m, etc., are constants to be determined. ϕ denotes the building block aspect ratio b/a, and $\lambda^2 = \omega a^2 \sqrt{\rho/D}$, the dimensionless driving frequency. Here, ρ denotes the mass per unit area and D the flexural rigidity of the building block.

The unknown spacial distribution of the imposed edge rotation is expressed in series form as

$$\left.\frac{\partial W(\xi, \eta)}{\partial \eta}\right|_{\eta = 1} = \sum_{m=0}^{\infty} E_m \cos m\pi\xi. \tag{5}$$

We wish to express the building block response in terms of the above Fourier driving coefficients, E_m.

It is immediately obvious that, due to the boundary conditions imposed along the edge, $\eta = 0$, all antisymmetric terms in equations (3) and (4) must vanish. This eliminates two unknown coefficients in each equation. Next, enforcing the condition of zero vertical edge reaction along the driven edge, we obtain the relationship [6]

$$-\left\{\frac{\partial^3 W(\xi, \eta)}{\partial \eta^3} + \nu^* \phi^2 \frac{\partial^3 W(\xi, \eta)}{\partial \eta \partial \xi^2}\right\}\Bigg|_{\eta = 1} = 0. \tag{6}$$

Substituting equation (1) into equation (6), it follows that we may write

$$Y'''(\eta) - \nu^* \phi^2 (m\pi)^2 Y'_m(\eta)|_{\eta = 1} = 0, \tag{7}$$

where the superscripts indicate differentiation with respect to η.

Substituting equations (3) and (4) (with second and fourth terms deleted) into equation (6), we obtain:
for $\lambda^2 > (\mathrm{m}\pi)^2$,

$$Y_m(\eta) = A_m\{\cosh \beta_m \eta + \theta_{1m} \cos \gamma_m \eta\} \tag{8}$$

and for $\lambda^2 < (m\pi)^2$,

$$Y_m(\eta) = A_m\{\cosh \beta_m \eta + \theta_{2m} \cosh \gamma_m \eta\}, \tag{9}$$

where

$$\theta_{1m} = -\frac{\beta_m(\beta_m^2 - \nu^* \phi^2 (m\pi)^2)\sinh \beta_m}{\gamma_m(\gamma_m^2 + \nu^* \phi^2 (m\pi)^2)\sin \gamma_m}, \qquad \theta_{2m} = -\frac{\beta_m(\beta_m^2 - \nu^* \phi^2 (m\pi)^2)\sinh \beta_m}{\gamma_m(\gamma_m^2 - \nu^* \phi^2 (m\pi)^2)\sinh \gamma_m}.$$

Finally, enforcing the boundary condition expressed by equation (5), and employing equations (1), (8), and (9), we obtain:
for $\lambda^2 > (m\pi)^2$,

$$Y_m(\eta) = E_m \theta_{11m}(\cosh \beta_m \eta + \theta_{1m} \cos \gamma_m \eta) \tag{10}$$

and for $\lambda^2 < (m\pi)^2$,

$$Y_m(\eta) = E_m\theta_{22m}\{\cosh\beta_m\eta + \theta_{2m}\cosh\gamma_m\eta\}, \tag{11}$$

where

$$\theta_{11m} = \frac{1{\cdot}0}{\beta_m\sinh\beta_m - \theta_{1m}\gamma_m\sin\gamma_m}, \qquad \theta_{22m} = \frac{1{\cdot}0}{\beta_m\sinh\beta_m + \theta_{2m}\gamma_m\sinh\gamma_m}.$$

It is important to note that with equations (10) and (11), we have made available the exact solution for the building block response to any harmonic edge rotation excitation.

We now wish to examine the building block (b) of Figure 1. It will be obvious that the solution for this building block may be extracted from that of building block (a) through a proper interchange of axes. We must, however, make certain additional observations. Not only must the variables ξ and η, related to the first solution, be interchanged but the aspect ratio ϕ must be replaced by its inverse $1{\cdot}0/\phi$, where $\phi = b/a$. Two further observations are important. Since the parameter λ^2 was based on edge length a, it must now be replaced by the product $\lambda^2\,\phi^2$ so that it is based on edge length b in the new formulation. Finally, it is important to note that the lateral displacement in the solution for building block (b) will be non-dimensionalized by edge length b. In summary, the solution for building block (b) is written as

$$W(\xi,\eta) = \sum_{n=0,1}^{\infty} Y_n(\xi)\cos n\pi\eta, \tag{12}$$

where for $\lambda^2\phi^2 > (n\pi)^2$,

$$Y_n(\xi) = E_n\theta_{11n}\{\cosh\beta_n\xi + \theta_{1n}\cos\gamma_n\xi\} \tag{13}$$

and for $\lambda^2\phi^2 < (n\pi)^2$,

$$Y_n(\xi) = E_n\theta_{22n}\{\cosh\beta_n\xi + \theta_{2n}\cosh\gamma_n\xi\} \tag{14}$$

and where $\beta_n^2 = \{\lambda^2\varphi^2 + (n\pi)^2\}/\phi^2$ and $\gamma_n^2 = \{\lambda^2\phi^2 - (n\pi)^2\}/\phi^2$ or $\{(n\pi)^2 - \lambda^2\varphi^2\}/\phi^2$ whichever is positive. Also,

$$\theta_{1n} = \frac{-\beta_n\{\beta_n^2 - \nu^*(n\pi)^2/\phi^2\}\sinh\beta_n}{\gamma_n\{\gamma_n^2 + \nu^*(n\pi)^2/\phi^2\}\sin\gamma_n}, \qquad \theta_{11n} = \frac{1{\cdot}0}{\beta_n\sinh\beta_n - \theta_{1n}\gamma_n\sin\gamma_n},$$

$$\theta_{2n} = \frac{-\beta_n\{\beta_n^2 - \nu^*(n\pi)^2/\phi^2\}\sinh\beta_n}{\gamma_n\{\gamma_n^2 - \nu^*(n\pi)^2/\phi^2\}\sinh\gamma_n}, \qquad \theta_{22n} = \frac{1{\cdot}0}{\beta_n\sinh\beta_n + \theta_{2n}\gamma_n\sinh\gamma_n}.$$

Note that the subscript n is used here for all the solutions where the analytical functions run in the x direction and $W(\xi,\eta)$ (equation (12)), for such solutions represents lateral displacement divided by edge length b.

The third building block in Figure 1 differs from the second in two ways only. Firstly, its edge, $\xi = 1$, has a condition of zero slope taken normal to the edge, enforced along its driven boundary. This condition is indicated by two solid dots joined across the edge. Secondly,

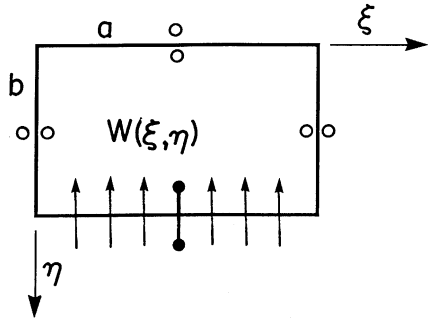

Figure 2. Schematic representation of intermediate building block.

the same edge is driven by a distributed, forced harmonic vertical edge reaction, also of circular frequency ω.

It is advantageous in seeking a solution for this building block to begin by obtaining a solution for the building block depicted in Figure 2.

Response for this latter building block is obtained in a fashion exactly analogous to that followed in obtaining the solution for the first building block of Figure 1. The procedure will not be repeated here. The displacement $W(\xi, \eta)$ and the functions $Y_m(\eta)$ again take the form of equations (1), (3), and (4) respectively. Distribution of amplitude of the harmonic vertical edge reaction is represented in the same series as utilized in equation (5). Solutions for the functions $Y_m(\eta)$ are expressed as:
for $\lambda^2 > (m\pi)^2$,

$$Y_m(\eta) = E'_m\theta'_{11m}\{\cosh\beta_m\eta + \theta'_{1m}\cos\gamma_m\eta\}, \tag{15}$$

and for $\lambda^2 < (m\pi)^2$,

$$Y_m(\eta) = E'_m\theta'_{22m}\{\cosh\beta_m\eta + \theta'_{2m}\cosh\gamma_m\eta\}, \tag{16}$$

where

$$\theta'_{1m} = \frac{\beta_m \sinh\beta_m}{\gamma_m \sin\gamma_m}, \qquad \theta'_{2m} = \frac{-\beta_m \sinh\beta_m}{\gamma_m \sinh\gamma_m},$$

$$\theta'_{11m} = \frac{-1{\cdot}0}{\beta_m^3 \sinh\beta_m + \theta'_{1m}\gamma_m^3 \sin\gamma_m}, \qquad \theta'_{22m} = \frac{-1{\cdot}0}{\beta_m^3 \sinh\beta_m + \theta'_{2m}\gamma_m^3 \sinh\gamma_m},$$

and where the single prime superscript is employed to avoid confusion with respect to the first building block. Quantities β_m and γ_m are, of course, as defined for the first building block of Figure 1.

A solution for building block (c) of Figure 1 is extracted from that given immediately above through a transformation of axes. It will take a form identical to that given by

equations (12)–(14). For this later solution, we find that

$$\theta'_{1n} = \frac{\beta_n \sinh \beta_n}{\gamma_n \sin \gamma_n}, \qquad \theta'_{2n} = \frac{-\beta_n \sinh \beta_n}{\gamma_n \sinh \gamma_n},$$

$$\theta'_{11n} = \frac{-1}{\beta_n^3 \sinh \beta_n + \theta'_{1n}\gamma_n^3 \sin \gamma_n}, \qquad \theta'_{22n} = \frac{-1}{\beta_n^3 \sinh \beta_n + \theta'_{2n}\gamma_n^3 \sinh \gamma_n},$$

where primes indicate equations pertaining to building blocks driven by harmonic vertical edge reactions.

In order to prepare for what is to follow, it is of utmost importance, at this time, to review the dimensionless formulation of bending moments and vertical edge reactions as they apply to the above building blocks. It was demonstrated in reference [6] that these quantities may be expressed as follows:

$$M_\eta = \frac{Mb^2}{aD}, \qquad V_\eta = \frac{Vb^3}{aD},$$

where

$$\frac{Mb^2}{aD} = -\left\{\frac{\partial^2 W(\xi,\eta)}{\partial \eta^2} + \nu\phi^2 \frac{\partial^2 W(\xi,\eta)}{\partial \xi^2}\right\} \tag{17}$$

and

$$\frac{Vb^3}{aD} = -\left\{\frac{\partial^3 W(\xi,\eta)}{\partial \eta^3} + \nu^*\phi^2 \frac{\partial^3 W(\xi,\eta)}{\partial \eta \partial \xi^2}\right\} \tag{18}$$

with M and V being the actual moments and vertical edge reactions, and subscript η refers to the η direction.

Similarly, for the ξ direction, we have:

$$M_\xi = \frac{Ma}{D}, \qquad V_\xi = \frac{Va^2}{D},$$

where

$$\frac{Ma}{D} = -\left\{\frac{\partial^2 W(\xi,\eta)}{\partial \xi^2} + \nu/\phi^2 \frac{\partial^2 W(\xi,\eta)}{\partial \eta^2}\right\} \tag{19}$$

and

$$\frac{Va^2}{D} = -\left\{\frac{\partial^3 W(\xi,\eta)}{\partial \xi^3} + \nu^*/\phi^2 \frac{\partial^3 W(\xi,\eta)}{\partial \xi \partial \eta^2}\right\}. \tag{20}$$

We should also recall at this time the definition of λ^2 and the fact that here the lateral displacement is non-dimensionalized through division by edge length a.

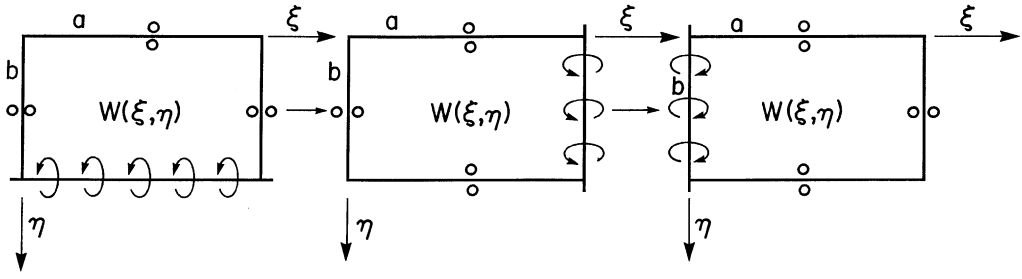

Figure 3. Schematic representation of intermediate building blocks and building block of ultimate interest.

In what follows, it will be important to note that equations (17)–(20) relating the bending moments and vertical edge reactions to lateral displacement will also be valid for response solutions with analytical functions running in the ξ direction, as described immediately above, provided we multiply the right-hand sides by the quantity b/a. This is necessary as the lateral displacement for these latter solutions is divided by edge length b.

The building block solutions (a)–(c) of Figure 1 above are the only ones required for the entire plate analysis, with the exception of the first plate segment beginning at the clamped edge. In order to satisfy the clamped edge conditions, four other building block solutions are required. They are represented schematically in Figure 1 and are denoted by the letters (d)–(g). Extended lines along the edges, $\xi = 0{\cdot}0$, indicate simple or hinged support.

Focusing first on building block (d), it is found that it is easiest to generate the required solution by proceeding as follows.

We begin by generating the solution for the response of the first building block of Figure 3. It is driven by a distributed harmonic edge rotation and its solution differs from that of building block (a) of Figure 1 only in that a condition of zero lateral displacement, rather than zero vertical edge reaction is enforced along the driven edge. The reader will have no trouble generating this solution. Immediately afterward, one can extract the solution for the second building block of Figure 3 from the first following the transformation rules discussed earlier. In fact, except for the quantities θ'_{1n} and θ'_{2n}, the solution will be identical to that given by equations (12)–(14). The quantities θ'_{1n} and θ'_{2n} become

$$\theta'_{1n} = -\cosh \beta_n / \cos \gamma_n, \qquad \theta'_{2n} = -\cosh \beta_n / \cosh \gamma_n.$$

Finally, the solution for the third building block of Figure 3, which is identical to the fourth building block (d) of Figure 1, is extracted from the solution presented immediately above by simply replacing the quantity ξ of the above solution with the quantity $1 - \xi$. In view of sign conventions, one must precede this solution with a negative sign.

Building block (e) of Figure 1 differs from (a) only in that now the edge, $\xi = 0{\cdot}0$, is given as simple support instead of slip–shear support. A Levy type solution for this latter problem is written as

$$W(\xi, \eta) = \sum_{m=1,2}^{\infty} Y_m(\eta) \sin (2m - 1)\pi\xi/2. \tag{21}$$

The quantities $Y_m(\eta)$ are immediately extracted from those derived for building block (a) of Figure 1 by simply replacing the quantity $m\pi$ of the earlier solution with the quantity $(2m - 1)\pi/2$.

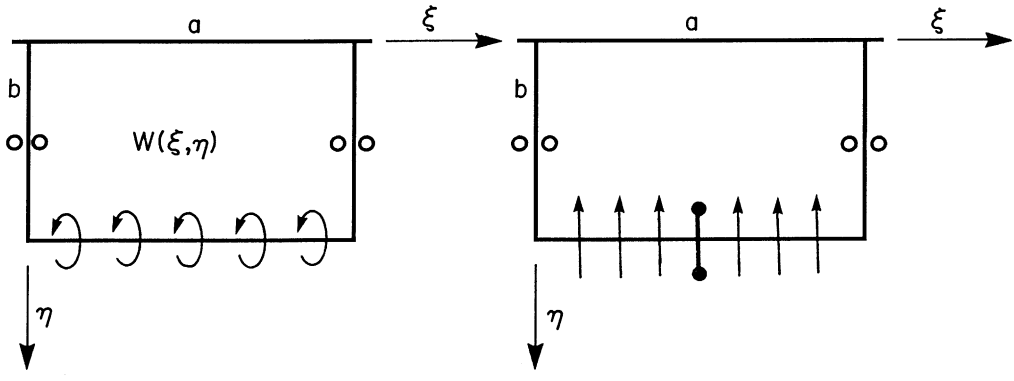

Figure 4. Schematic representation of additional intermediate building blocks.

In order to obtain the solution (f) of Figure 1, it is wise to begin by obtaining the solution for the first building block of Figure 4. This building block differs from the first of Figure 1 only in that a simple support, rather than a slip–shear condition, is imposed along the edge, $\eta = 0$. The solution will take the form of equation (1); however, we must now delete the symmetric terms rather than the antisymmetric terms of equations (3) and (4). Following steps analogous to those described in detail for the earlier building block, it is found that quantities β_m and γ_m are unchanged; however, the quantities $Y_m(\eta)$ now become:
for $\lambda^2 > (m\pi)^2$,

$$Y_m(\eta) = E_m\theta_{11m}\{\sinh\beta_m\eta + \theta_{1m}\sin\gamma_m\eta\}, \tag{22}$$

and for $\lambda^2 < (m\pi)^2$,

$$Y_m(\eta) = E_m\theta_{22m}\{\sinh\beta_m\eta + \theta_{2m}\sinh\gamma_m\eta\}, \tag{23}$$

where

$$\theta_{1m} = \frac{\beta_m\{\beta_m^2 - v^*\phi^2(m\pi)^2\}\cosh\beta_m}{\gamma_m\{\gamma_m^2 + v^*\phi^2(m\pi)^2\}\cos\gamma_m}, \qquad \theta_{2m} = \frac{-\beta_m\{\beta_m^2 - v^*\phi^2(m\pi)^2\}\cosh\beta_m}{\gamma_m\{\gamma_m^2 - v^*\phi^2(m\pi)^2\}\cosh\gamma_m},$$

$$\theta_{11m} = \frac{1{\cdot}0}{\beta_m\cosh\beta_m + \theta_{1m}\gamma_m\cos\gamma_m}, \qquad \theta_{22m} = \frac{1{\cdot}0}{\beta_m\cosh\beta_m + \theta_{2m}\gamma_m\cosh\gamma_m}.$$

The solution for the response of building block (f) is, of course, extracted from the solution immediately above through a transformation of axes as already discussed.

A solution for building block (g) of Figure 1 is obtained in an analogous fashion. One begins with the second building block of Figure 4. It differs from the building block of Figure 2 only in that simple support is enforced at the edge, $\eta = 0$. Again, the solution will take the form of equation (1) with the functions $Y_m(\eta)$ as expressed by equations (22) and (23).

The quantities θ_{1m}, etc., become

$$\theta_{1m} = \frac{-\beta_m\cosh\beta_m}{\gamma_m\cos\gamma_m}, \qquad \theta_{2m} = \frac{-\beta_m\cosh\beta_m}{\gamma_m\cosh\gamma_m}, \qquad \theta_{11m} = \frac{-1{\cdot}0}{\beta_m^3\cosh\beta_m - \theta_{1m}\gamma_m^3\cos\gamma_m},$$

and

$$\theta_{22m} = \frac{-1{\cdot}0}{\beta_m^3 \cosh \beta_m + \theta_{2m}\gamma_m^3 \cosh \gamma_m}.$$

Finally, the above solution must be given a transformation of axes to provide the solution for the response of building block (g).

The required building block solutions are now available for the analysis of the entire cantilever plate with discontinuities in properties.

2.2. GENERATION OF THE EIGENVALUE MATRIX

We choose here, for illustrative purposes, to describe the generation of the eigenvalue matrix for a cantilever plate with two discontinuities in properties. This implies that the plate is composed of three distinct segments. It will be seen that the analytical procedure is valid regardless of the number of discontinuities in plate properties.

We wish to keep the approach general by permitting the dimension a of the individual plate segments to take on any desired value. It is convenient in any study, therefore, to express the reference value for the dimensionless frequency as λ_b^2, where the frequency is non-dimensionalized through the use of the edge length b. While length a may change from span to span, length b remains constant.

We also accept that each segment may have different values for effective mass per unit area and plate flexural rigidity. The practice followed there is to base the reference quantity, λ_b^2, on the mass per unit area, and flexural rigidity, of the first segment of the plate i.e., the segment bounded by the clamped edge.

It follows, therefore, that for any segment, let us say segment i, the associated quantity λ_a^2 becomes

$$\lambda_a^2 = \{\lambda_b^2/\phi_i^2\} R_i, \quad R_i = \sqrt{\frac{\rho_i/D_i}{\rho_1/D_1}}. \tag{24, 25}$$

Here, the subscript 1 refers to the first segment, and ρ and D are the mass per unit area, and flexural rigidity, respectively, of the segment to which the subscript i refers. On moving to each new segment, equation (24) is utilized to establish the related value of λ_a^2.

In order to conduct a free vibration analysis of a cantilever plate of three distinct segments, a sequence of building blocks as depicted along the top of Figure 5 is required. The digit appearing inside each building block outline indicates the plate segment to which it pertains. We denote the number of terms utilized in the series solution of each building block by K. Figure 5 is a schematic representation of the eigenvalue matrix, where the value of K has been arbitrarily set equal to 3. The unknown driving coefficients associated with the various building blocks, e.g., $E_{n1}(i)$, $i = 1, 2, 3$, $E_{m1}(i)$, $i = 1, 2, 3$, etc., are listed immediately beneath the building blocks of the figure. This practice has been followed in numerous publications employing the superposition method.

It will be noted that while there are 16 building blocks in the figure, there are only 12 sets of driving coefficients. This is because four adjacent pairs of building blocks form "coupled pairs". It will be shown that driving coefficients associated with the building blocks of each pair are not independent but differ by a fixed multiplying factor.

Since we have 12 sets of driving coefficients to constrain, we must also have 12 sets of boundary conditions, or inter-plate segment continuity conditions, to enforce. These

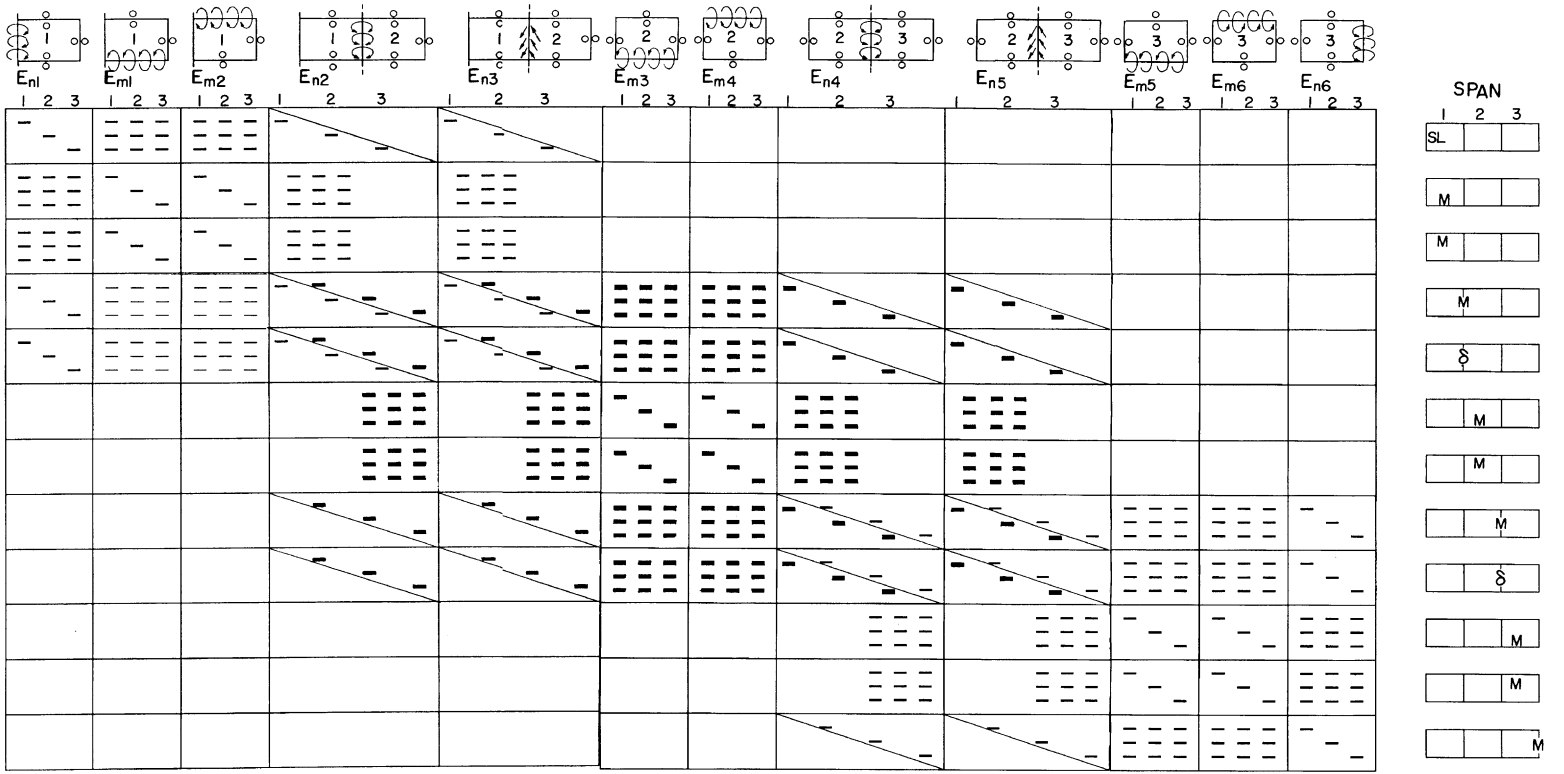

Figure 5. Schematic representation of eigenvalue matrix for analyzing cantilever plate of three distinct segments ($K = 3$). Heavier bars indicate matrix elements associated with the intermediate plate segment.

boundary/continuity conditions are represented schematically by insets along the right-hand side of the figure. Numbers along the top of these insets indicate the plate segment to which reference is made. The first inset indicates, for example, that a condition of zero slope along the clamped edge of the first plate segment must be satisfied. The second and third insets indicate edges along which a condition of zero bending moment must be enforced. The fourth inset indicates that a condition of continuity of bending moment along the interface of the first and second plate segments must be enforced, etc.

Well-established practices are followed in generating the eigenvalue matrix for problems undergoing analysis by means of the superposition method. In the present problem, we must develop a set of $12K$ homogeneous algebraic equations relating the $12K$ unknown driving coefficients. The eigenvalue matrix consists of the coefficient matrix for this set of equations.

For illustrative purposes, we will begin by examining the first row of matrix segments of Figure 5 which arise from imposing the condition of zero slope along the plate clamped edge. It is agreed that only building blocks of the first plate segment contribute toward this slope. Furthermore, solutions for the response of each of these five building blocks exist. Solutions for the first, fourth, and fifth building blocks are those of the building blocks depicted in Figure 1(d), 1(f), and 1(g). The solution for the second building block is available from that of Figure 1(e). The solution for the third building block is also available from that of Figure 1(e) in replacing the quantity η with $(1 - \eta)$.

Standard procedures are employed to enforce the prescribed boundary conditions. The contributions of all the building blocks toward the slope along the edge, $\xi = 0{\cdot}0$, of the first plate segment are expanded in an appropriate trigonometric series and the net coefficient of each term in the new series is set equal to zero. This gives rise to a set of K homogeneous algebraic equations relating the driving coefficients E_{n1}, E_{m1}, etc. It is found advantageous here to choose the cosine series of equation (1) for the expansion, since contributions to the slope of three of the building blocks already exist in terms of this series. Short bars in the first row of matrix segments indicate the coefficients in the set of equations thus obtained.

Two points should be made clear at this time. Firstly, we wish to express the slope as $\partial W(\xi, \eta)/\partial\xi$, where $\xi = 0{\cdot}0$, $W(\xi, \eta)$ equals lateral displacement divided by segment width a. Since displacement for the first, fourth, and fifth building blocks of the first plate segment is non-dimensionalized through division by edge length b, each contribution toward the slope of these building blocks must be multiplied by the plate segment aspect ratio ϕ_1 in order to preserve consistency.

Secondly, it will be noted that matrix elements appearing in the first row of segments immediately beneath the coupled building blocks (discussed earlier) lie along, but to the left of, a diagonal line drawn through the segment. This is to indicate that these diagonal elements pertain to the left building block of the coupled pair. When such diagonal elements pertain to the right building block of the coupled pair, they will appear to the right of the diagonal line.

Moving down to the second row of segments of the matrix (Figure 5), it is seen that we must now expand the contributions of building blocks toward bending moment along the edge, $\eta = 1$, of the first plate segment in an appropriate series. Here, it is advantageous to utilize the sine series of equation (21) as contributions of two of the building blocks are available in the form of this series. The required bending moment is, of course, obtained from equation (17). It is pointed out again that when applying this equation to building block solutions with lateral displacement non-dimensionalized through edge length b, the results must be multiplied by the aspect ratio of the plate segment involved. An identical procedure permits the generation of matrix elements of the third row of segments.

The fourth row of segments arises because of the need to enforce the condition of continuity of bending moment at the interface of the first and second plate segments. All building blocks of the first and second plate segments will contribute toward the moment at the interface. The practice here is to enter moment contributions toward the left-hand side of the interface as positive and those contributing to the right-hand side as negative, thus keeping the constraining equations in regular homogeneous form.

Before discussing matrix elements associated with this continuity condition further, it is appropriate to discuss the driving coefficients associated with the first two coupled pairs of building blocks in the set. We begin by focusing on the first pair. Each building block is driven by a harmonic edge rotation.

In the interest of generality, we will denote the successive building blocks in each coupled pair by the subscripts i and j respectively. Since the two building blocks in the pair under consideration are the only ones that can contribute toward slope at their interface, actual slopes must be equal at this location. We denote the first driving coefficient as E_n and the second as E_n^*.

For building blocks i and j, actual slopes at the interface become, respectively,

$$\left.\frac{\partial W(\xi,\eta)}{\partial \xi}\right|_{\xi=1} b/a_i = E_n b/a_i \tag{26}$$

and

$$\left.\frac{\partial W(\xi,\eta)}{\partial \xi}\right|_{\xi=0{\cdot}0} b/a_j = -E_n^* b/a_j. \tag{27}$$

At any such interface, we may therefore write

$$E_n^* = E_n\{-\phi_i/\phi_j\}. \tag{28}$$

All the matrix elements related to the second building block of coupled pairs of this type must be pre-multiplied by the factor on the right-hand side of the above equation.

We turn next to the first transverse force-driven pair of coupled building blocks. This time it is recognized that the actual transverse shear forces must be continuous across the interface of the pair. Again, employing the subscripts i and j, we write

$$\left.\frac{Va_i^3}{bD_i}\right|_{\xi=1} = E_n \tag{29}$$

and

$$\left.\frac{Va_j^3}{bD_j}\right|_{\xi=0{\cdot}0} = -E_n^*, \tag{30}$$

where the subscript n has again been utilized to indicate the driving coefficient. The quantities on the left-hand side of the equations (29) and (30) represent non-dimensional vertical edge reaction after the transformation of the solution of Figure 2 (equation (18)).

It follows immediately that we may write

$$E_n^* = E_n\{-(D_i/D_j)[\phi_i/\phi_j]^3\}. \tag{31}$$

Here, of course, D_i and D_j are the flexural rigidities of the respective plate segments.

Again, all matrix elements related to the second building block of the pair must be pre-multiplied by the factor on the right-hand side of equation (31).

Returning now to the fourth row of matrix segments, it is found appropriate to expand all building block contributions toward bending moment at the interface of the first and second plate segments in a cosine series. Bending moments are obtained for each building block according to equation (19), and we recall that all the expansions developed for building blocks with analytical functions running in the ξ direction must be multiplied by the aspect ratio of the plate segment involved. All contributions to the left-hand side of the interface are entered as positive.

The same practice is followed in entering contributions to the right-hand side of the interface, except that these must be entered as negative. One other consideration is important. Again, denoting successive plate segments, beginning at the left-hand side of the interface, by the subscripts i and j, respectively, it is seen that for the left-hand side of the interface, equation (19) provides the quantity Ma_i/D_i. While, for the right-hand side, it gives the quantity Ma_j/D_i. Since we wish to enforce the continuity of actual moment, M, we must multiply matrix elements to the right-hand side of the interface by the quantity $\phi_j D_j/\phi_\ell D_i$.

The fifth row of matrix segments arises because of the need to enforce a condition of continuity of plate lateral displacement across the above interface. All the lateral displacements must be non-dimensionalized throughout the row of segments by the same length. Here it has been found convenient to non-dimensionalize all the displacements through division by edge length b. Since displacements for solutions with analytical solutions running in the ξ direction are already non-dimensionalized in this manner, no multiplication factor is required. Displacements obtained from the other solutions, for any segment i, must be divided by the quantity ϕ_i.

The remainder of the matrix is generated following the procedures already described. The only exception relates to the final row of matrix segments where a condition of zero net-bending moment along the plate outer edge must be enforced.

It will be noted in Figure 5 that matrix elements related to the second, or central, plate segment are designated by heavier bars. This is done for the convenience of the reader. It will be recognized that with a cantilever plate of four distinct spans, for example, this central portion of the matrix associated with the second plate segment will have to be augmented with a similar section downward and to the right and associated with the third plate segment. The final portion of the matrix will then be associated with the fourth and final plate segment.

It is important to point out here that once a computer routine has been written for the three-segment plate, it is easy to index the routine so that it can handle plates of any number of segments. This has in fact been done. With four distinct plate segments, the associated matrix will comprise an array of segments, 16×16, instead of the 12×12 array associated with the three-segment plate.

3. PRESENTATION OF COMPONENT RESULTS

Fortunately, a number of convincing tests can be performed in order to verify the theoretical model described and the computer routine utilized to generate the eigenvalue matrix and establish the eigenvalues.

All eigenvalues are computed by following well-established procedures. With all the parameters of the problem selected, a trial eigenvalue, λ_b^2, is also selected and the associated matrix is generated. The determinant of the matrix is computed, the trial eigenvalue is augmented, and the process repeated. Eigenvalues are those values of the parameter, λ_b^2,

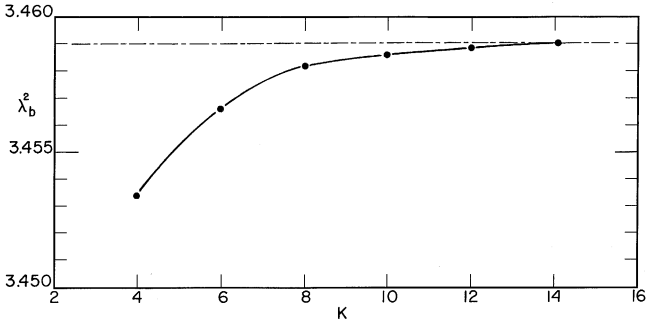

Figure 6. Computed eigenvalue versus parameter K for square cantilever plate of three equal segments, with identical properties. Broken line indicates known eigenvalue for classical square cantilever plate.

which cause the determinant of the matrix to vanish. Mode shapes are obtained by setting one of the non-zero driving coefficients equal to unity and solving the resulting set of non-homogeneous algebraic equations relating to the remaining driving coefficients. With all the coefficients established, the plate mode shape associated with the eigenvalue is generated.

As a first verification test, a square cantilever plate was examined. It is known that the eigenvalue for this problem, with uniform properties throughout, is $=3{\cdot}459$. The same plate was examined using the present analytical approach. It was considered to be composed of three equal segments; however, for this test the properties of all the segments were treated as being equal, thus an eigenvalue of 3·459 was to be anticipated.

Results of the study are presented in Figure 6. It is seen that the computed eigenvalue for the three-segment plate converges rapidly to the known limiting value. With 12 terms utilized in the building block solution series, there is an agreement to four significant digits. Similar tests were conducted with the plate divided into four equal segments for both square and non-square plates. Good convergence to known eigenvalues was obtained.

In a further test, similar to that described above for the square plate, the first and second plate segments, moving out from the clamped edge, were allowed to take on different aspect ratios, the new aspect ratios thus specified, however, that the overall plate was still square. One therefore anticipated no change in computed eigenvalue, regardless of the pairs of aspect ratios assigned to the first and second plate segments, within the above constraints. This, in fact, was found to be the case.

It will be appreciated that no comprehensive set of eigenvalues could be prepared to cover the range of plate geometries and property discontinuities which might be encountered in problems of the type considered here. The best that can be done is to present computed results of a limited scope which will provide other researchers and designers with data against which their computed results can be compared.

Toward this end, we first present the results of a study of a square cantilever plate composed of three segments of equal geometry but of different structural properties. A plate with two-step discontinuities in thickness has been selected for this purpose. An edge view of a plate of this type is shown schematically in Figure 7.

While only the ratio of plate segment thicknesses to that of the first segment is required, it was decided, for convenience, to assign actual thicknesses to each segment. These thicknesses are seen to be 1/2 in (1·270 cm), 3/8 in (0·9525 cm), and 1/4 in (0·6350 cm) as we move out from the clamped edge.

It will be recalled that the mass per unit area of each segment is proportional to the segment thickness, h. Furthermore, flexural rigidity of each segment is proportional to h^3.

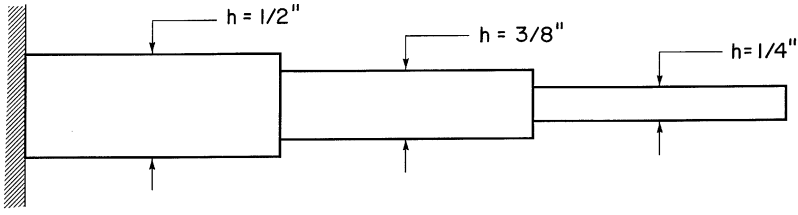

Figure 7. Edge view of a square cantilever plate of three segments of equal width but different thicknesses (not to scale).

TABLE 1

Eigenvalues computed for a square plate with two step discontinuities in thickness $(\lambda_b^2 = \omega b^2\sqrt{\rho/D_1})$

Mode	Eigenvalue λ_b^2	Type
1	4·132	Sym
2	7·597	Antisym
3	16·51	Sym
4	18·76	Sym

TABLE 2

Eigenvalues computed for plate of aspect ratio 3/4 *with three discontinuities in thickness* $(\lambda_b^2 = \omega b^2\sqrt{\rho/D_1})$

Mode	Eigenvalue λ_b^2	Type
(1)	2·572	Sym
(2)	4·877	Antisym
(3)	7·734	Sym
(4)	10·72	Antisym
(5)	11·14	Sym
(6)	17·58	Sym

The mass per unit area ratios of the second and third segments then become $\rho_2/\rho_1 = 3/4$ and $\rho_3/\rho_1 = 1/2$. Corresponding ratios for flexural stiffness of the segments become $D_2/D_1 = 27/64$ and $D_3/D_1 = 1/8$. The aspect ratio for each plate segment becomes 3·0.

The computed eigenvalues, λ_b^2, for the first four free vibration modes of this plate with two discontinuities in thickness are tabulated in Table 1. All modes must be symmetric, or antisymmetric, with respect to the plate center line running normal to the clamped edge. The type of mode associated with each eigenvalue is indicated on the right-hand side of the table.

The first six eigenvalues and mode shapes were computed for another plate of interest. This second plate had a clamped edge length of 12 in (30·48 cm), the other edge being 16 in (40·64 cm) in length, and the overall aspect ratio being equal to 3/4. It was divided into four segments of equal width (4 in), the first three segments having thicknesses identical to those given in Figure 7. The final outward segment had a thickness of 1/8 in (0·3175 cm). Computed eigenvalues for this plate are presented in Table 2. The type of mode (symmetric or antisymmetric) is also indicated.

Computed mode shapes for this four-segment plate are found in Figures 8–13.

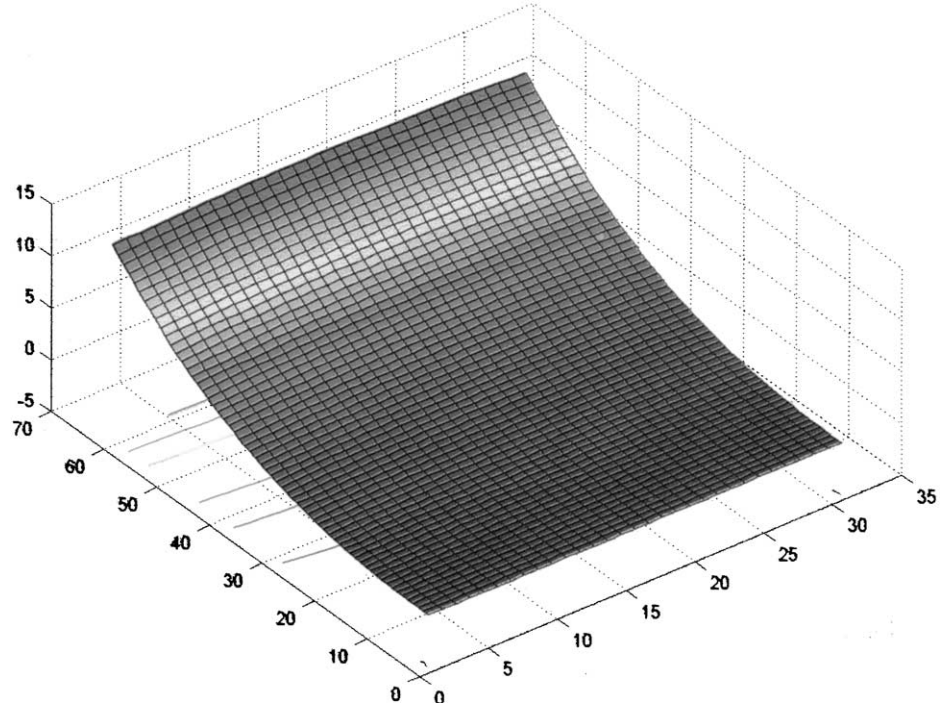

Figure 8. Computed first mode shape (plate of Table 2).

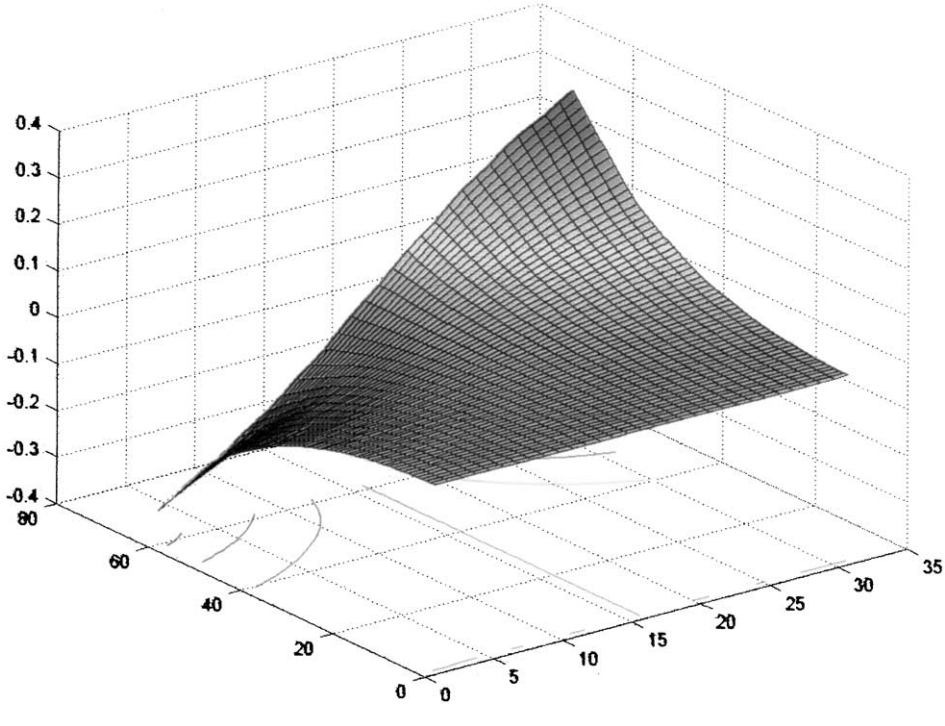

Figure 9. Computed second mode shape (plate of Table 2).

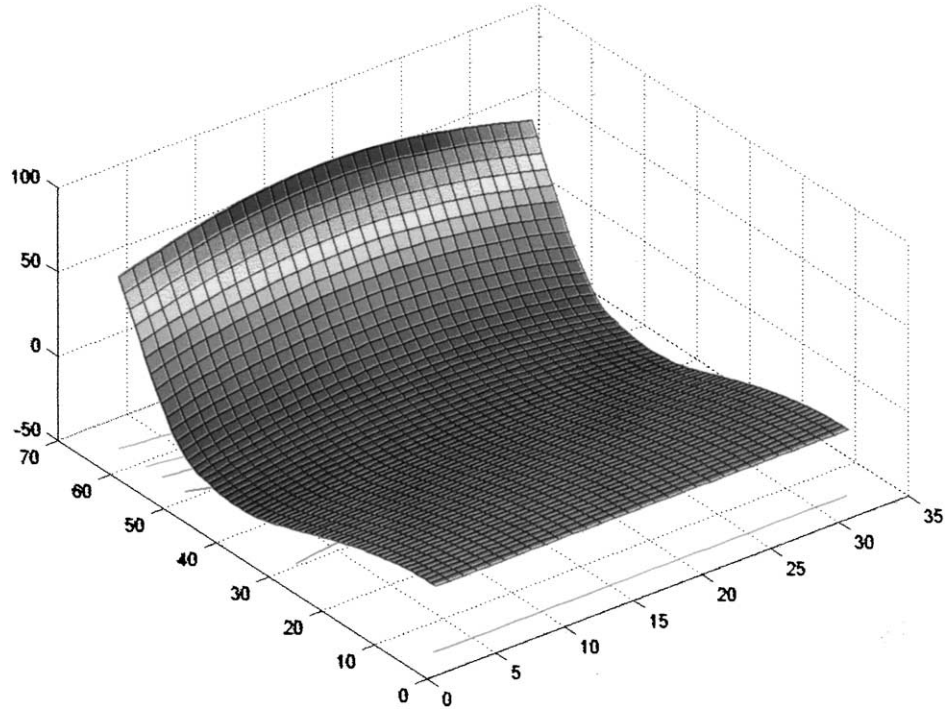

Figure 10. Computed third mode shape (plate of Table 2).

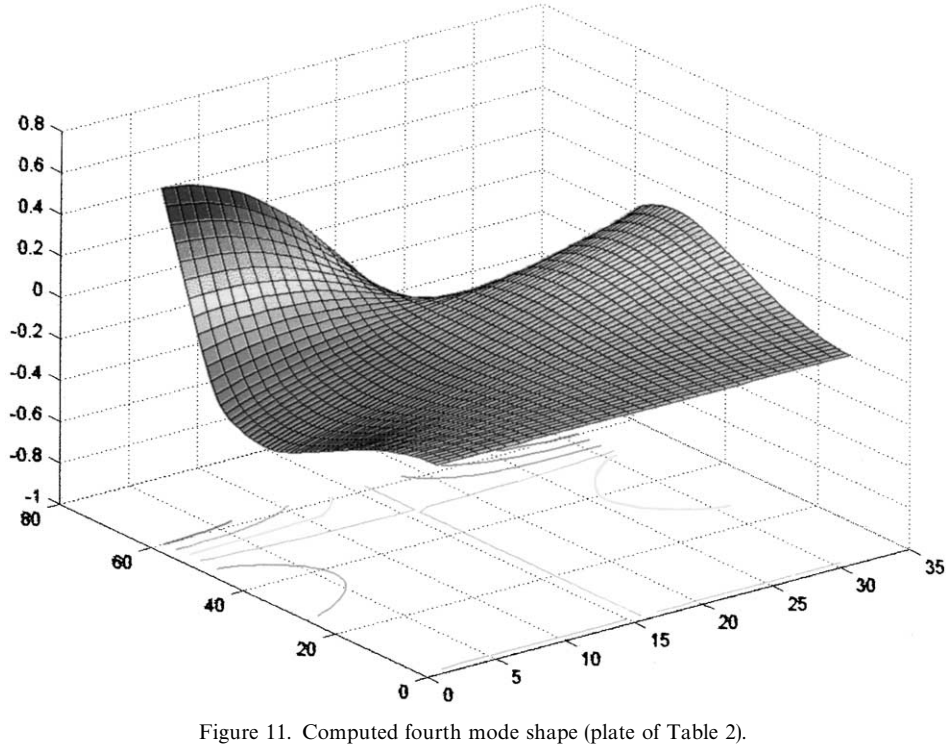

Figure 11. Computed fourth mode shape (plate of Table 2).

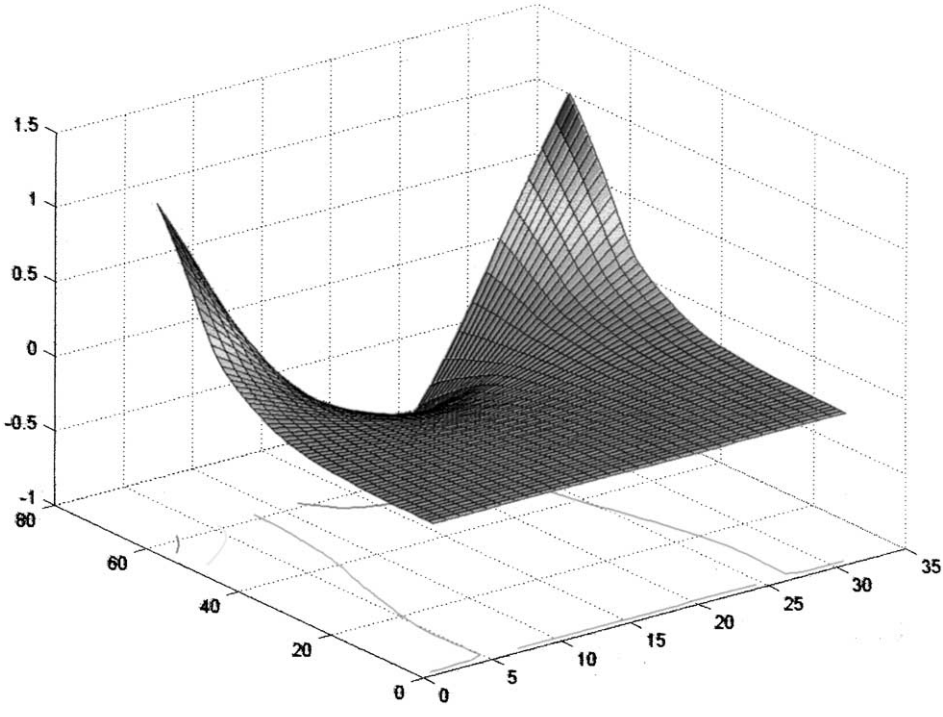

Figure 12. Computed fifth mode shape (plate of Table 2).

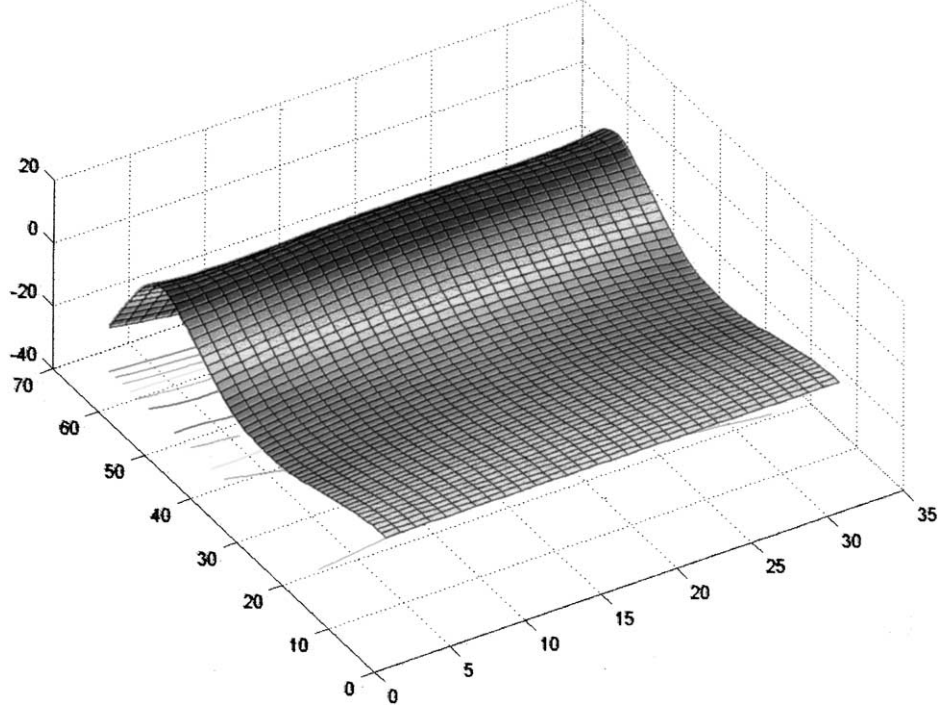

Figure 13. Computed sixth mode shape (plate of Table 2).

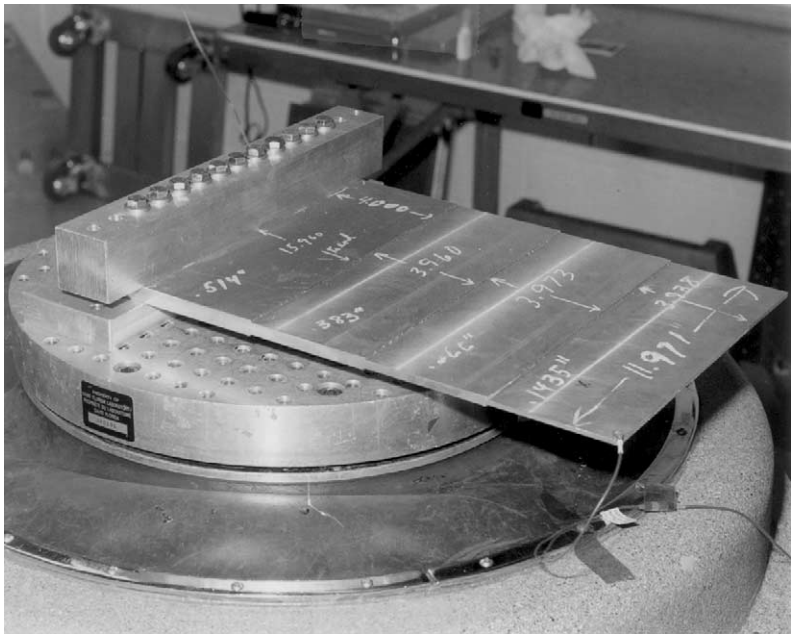

Figure 14. View of experimental test plate mounted on shaker test facility.

TABLE 3

Comparison between theoretical and experimentally measured free vibration frequencies for test plate with three step discontinuities in thickness

Mode	Type	Theoretical frequency (Hz)	Experimental frequency (Hz)
1	Sym	85·80	86·7
2	Antisym	167·0	166·0
3	Sym	278·2	269·0
4	Antisym	385·4	374·0
5	Sym	399·6	393·7
6	Sym	633·2	611·2

An experimental study of the free vibration behavior of a rectangular aluminum test plate with geometry and discontinuities identical to those described for the plate immediately above was carried out. The objective was to provide experimental results against which computed frequencies could be compared.

The test plate was machined from T6061 aluminum. It was mounted on an MB C-150 shaker by means of a special fixture. A view of this plate mounted on the shaker facility is to be found in Figure 14. During tests, a low level (0·5**g**) sine sweep at the sweep rate of 0·5 octaves/min was performed for the frequency bandwidth of 20–700 Hz.

To calculate eigenvalues and frequencies, the actual plate dimensions (segment widths and thicknesses, etc.) were used. These varied only slightly from the nominal dimensions given above. Fifteen terms were utilized for building block solutions in the theoretical analysis.

Measured and computed frequencies for the first six free vibration modes of this plate are presented in Table 3. It will be noted that the computed and experimentally measured

frequencies agree to within 3·5% or less. This is considered to be a very good agreement for studies of this type. It is known that it is difficult to achieve idealized clamping conditions along the fixed edge of the plate. It will also be noted that for almost all the modes, the theoretical frequencies are slightly higher than those measured experimentally. This is to be expected in view of the difficulty in achieving idealized clamping conditions.

4. DISCUSSION AND CONCLUSIONS

The superposition method is found highly suitable for obtaining analytical type solutions for the free vibration of cantilever plates with step discontinuities in plate properties. A number of verification tests have been performed through maintaining the multi-plate segment solution and letting plate properties take on uniform values throughout. Excellent agreement with known eigenvalues was obtained. These tests were followed by comparisons made between computed frequencies and those obtained experimentally. Agreement achieved in these latter tests can be described as very good. Tabulated eigenvalues provide other researchers with results against which they may compare their findings.

The reader will now appreciate, as pointed out earlier, that with the proper choice of building blocks, plates with any combinations of classical boundary conditions can be analyzed. It is also perhaps worth noting that some analysts might prefer to generate all segments of the eigenvalue matrix, beyond the segment related to the first plate span, as intermediate segments. It would then only be necessary to post-modify the segment related to the final span such that outer boundary conditions are satisfied.

The objective of obtaining an accurate analytical type solution for the problem under consideration has been achieved.

ACKNOWLEDGMENTS

Experimental work was carried out at the David Florida Laboratory of the Canadian Space Agency in Ottawa. The authors would like to acknowledge the valuable assistance of Tony Russiello in carrying out the experimental tests.

REFERENCES

1. J. L. San Emeterio, J. A. Gallego-Jurez and G. Rodriguez-Corral 1987 *Journal of Sound and Vibration* **114**, 495–505. High axisymmetric modes of vibration of stepped circular plates.
2. I. E. Harik, X. Liu and N. Balakrishnan 1992 *Journal of Sound and Vibration* **153**, 51–62. Analytical solution to free vibration of rectangular plates.
3. L. Jinkyo and L. A. Bergman 1993 *Vibration and Control of Mechanical Systems, American Society of Mechanical Engineers* **DE-61**, 243–256. Free and forced vibration of stepped levy plates.
4. J. Lee and L. A. Bergman 1944 *Journal of Sound and Vibration* **171**, 617–640. The vibration of stepped beams and rectangular plates by an elemental dynamic flexibility method.
5. F. L. Liu and K. M. Liew *Journal of Vibration and Acoustics—Transactions of the American Society of Mechanical Engineers* **121**, 204–208. Vibration analysis of discontinuous Mindlin plates by differential quadrature element method.
6. D. J. Gorman 1982 *Free Vibration Analysis of Rectangular Plates*. New York: Elsevier, North-Holland Co.

APPENDIX A: NOMENCLATURE

a	building block edge dimension
a_i	edge dimension of plate segment i

b	plate dimension along clamped edge
D	flexural rigidity of plate segment
D_i	flexural rigidity of plate segment i
E	modulus of elasticity of plate material
h	plate thickness
h_i	thickness of plate segment i
K	no. of terms utilized in building block solutions
w	plate lateral displacement
W	dimensionless plate lateral displacement
x, y	distances along plate edges
ν	the Poisson ratio of plate material
ν^*	$(= 2 - \nu)$
ξ	$(= x/a$, or $x/a_i)$
η	$(= y/b)$
ω	circular frequency of vibration
ρ_i	mass per unit area of segment i
ρ	mass per unit area of segment adjacent to clamped edge
λ^2	$(= \omega a_i^2 \sqrt{\rho/D_i})$ dimensionless frequency
λ_b^2	eigenvalue $= \omega \mathrm{b}^2 \sqrt{\rho/D_1}$